Article

Photocatalytic Degradation of Dichloroacetic Acid. A Kinetic Study with a Mechanistically Based Reaction Model

Mari#a de los Milagros Ballari, Orlando O. Alfano, and Alberto E. Cassano

Ind. Eng. Chem. Res., **2009**, 48 (4), 1847-1858• DOI: 10.1021/ie801194f • Publication Date (Web): 22 January 2009

Photocatalytic Degradation of Dichloroacetic Acid. A Kinetic Study with a Mechanistically Based Reaction Model

María de los Milagros Ballari,* Orlando O. Alfano, and Alberto E. Cassano

INTEC (Universidad Nacional del Litoral and CONICET), Colectora de la Ruta Nacional No. 168, Km 472.5, Edificio INTEC I, (3000) Santa Fe - Argentina

In the present work, a study of the reaction kinetics of the photocatalytic degradation of dichloroacetic acid (DCA) employing UV radiation and titanium dioxide suspensions is reported. This study involved the development of a kinetic model from a proposed complete reaction sequence and estimation of the kinetic parameters from experimental data. The experimental data were obtained using a perfect mixed photoreactor, because the operating conditions were chosen in compliance with restrictive conditions established in a previous work in which the possibility of mass-transfer limitations in slurry reactors was investigated. The significant variables in this study were (1) the initial DCA concentration, (2) the catalyst loading, and (3) the light intensity. Simulation results from the complete reactor mass balance, including radiation transport in the bulk and resistances inside the catalytic particle agglomeration, are in good agreement with experiments, which provides confidence in the estimation of the kinetic parameters within the range of the explored variables.

1. Introduction

Photocatalytic processes constitute one of the advanced oxidation technologies (AOTs) applied to water and air purification. These processes involve a solid semiconductor catalyst, typically titanium dioxide, which is activated with ultraviolet light of the appropriate wavelength. For various reasons repetitively reported, titanium dioxide has been the preferred choice.[1] These reactions are very attractive for treating pollution problems because (1) they transform pollutants into innocuous products in the vast majority of cases[2−4] and (2) they have very low selectivities, thus permitting the treatment of a wide range of contaminants including herbicides,[5] pesticides,[6,7] phenol and its derivatives,[8−10] halocarbonated compounds,[11,12] alcohols,[13,14] organic acids,[15−17] dyes,[18,19] nitrogen oxides,[20] cyanobacterial toxins,[21] and endocrine disruptors.[22]

Dichloroacetic acid (DCA) is a pollutant with environmental and clinical toxicological effects. This contaminant is a byproduct of water chlorination and a metabolite of other chlorinated compounds that are present in industrial effluents, such as trichloroacetic acid and perchloroethylene. It is considered a potential human carcinogenic as well.

Dichloroacetic acid is a model contaminant that presents some advantages for laboratory studies because of its low vapor pressure and high water solubility. In addition, the photocatalytic mineralization of DCA in aqueous media does not yield stable organic intermediates, simplifying the kinetic model. To date, DCA has been used as a model pollutant in several photocatalytic degradation studies with TiO_2.[23−27]

The photocatalytic degradation kinetic of DCA employing titanium dioxide suspensions was studied by Zalazar et al.,[28] who proposed a photocatalytic mineralization mechanism and a kinetic expression for the reaction rate with the intention of providing intrinsic parameters. Unfortunately, some of the experimental operating conditions and some of the assumptions made in the derivation of the kinetic model induced some objections to the results. Accordingly, this study differs significantly from the previous work, leading to a new and different kinetic study of this contaminant. The main differences between the two contributions are as follows: (1) The pH of the initial contaminated solution differed. Whereas Zalazar et al.[28] worked with pH values between 4 and 5, in the present work, higher DCA concentrations were employed, and consequently, the pH was significantly lower. The use of different pH values in a photocatalytic reaction has two main effects: (a) an alteration of the suspension characteristics at low pH, because of the formation of agglomerates, and (b) a modification in the affinity between the contaminant and the titanium dioxide surface, because the latter's charge is a function of the solution pH. (2) A change in the morphology of the catalyst led to changes in the optical properties, which are affected by the suspension pH.[29,30] (3) Better information concerning the phase function for inscattering is now available and was used in this work. Whereas Zalazar et al.[28] assumed an isotropic phase function, in this work, the Henyey−Greenstein (HG) phase function was utilized.[29] The HG phase function has the advantage of having an adjustable asymmetry factor that indicates whether the scattering is isotropic or directed forward or backward and adjusts calculations closer to the actual photon scattering distribution. (4) The thickness of the reactor used in this work is different from that used by Zalazar et al.;[28] therefore, the optical thicknesses of the two photoreactors contrast significantly for the same catalyst loading. It has been shown that this change could force the use of a very complete and rigorous representation of the radiation absorption rate.[31] (5) There are some important differences in the kinetic models of the two model approaches. Whereas the reaction rate was modeled in terms of a heterogeneous system in this work, in Zalazar et al.,[28] a simplification was made with respect to the system, considering its behavior to be pseudohomogeneous. This leads to different assumptions about the adsorption equilibrium of the pollutant on the catalytic surface. In addition, eq 8 in Zalazar et al.[28] relied on an implicit approximation that could lead to theoretical objections. (6) The material used in the reactor windows for the radiation entrance was different. In Zalazar et al.,[28] quartz plates were used, whereas in this work, borosilicate glass was employed. This resulted in a radiation wavelength distribution inside the photoreactor that was appreciably different because borosilicate glass just starts to transmit significant

* To whom correspondence should be addressed. E-mail: ballari@santafe-conicet.gov.ar. Tel.: +54 (0)342-4511546. Fax: +54 (0)342-4511087.

10.1021/ie801194f CCC: $40.75
Published on Web 01/22/2009

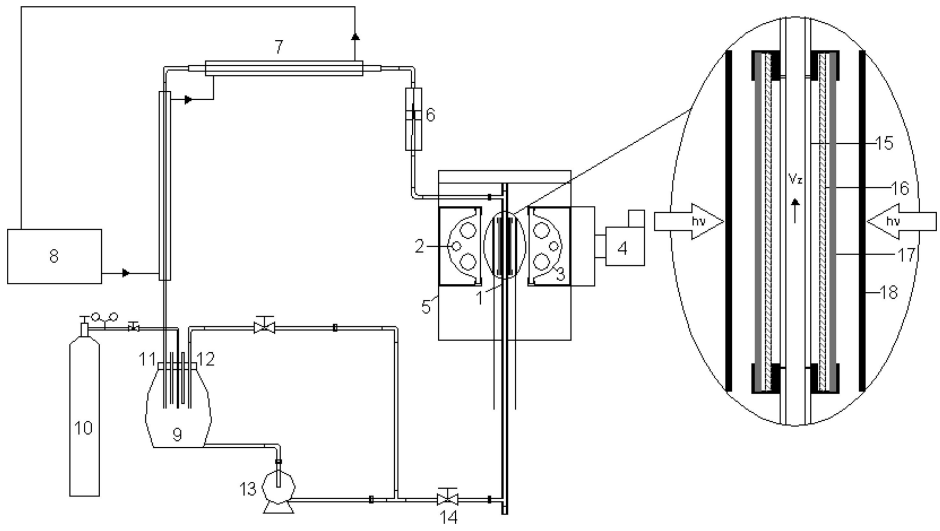

Figure 1. Reactor description. Key: (1) reactor, (2) UV lamp, (3) parabolic reflector, (4) fan, (5) box, (6) flowmeter, (7) heat exchanger, (8) thermostatic bath, (9) tank, (10) oxygen supply, (11) sampling, (12) thermometer, (13) pump, (14) valve, (15) borosilicate glass window, (16) borosilicate ground glass, (17) neutral filter, (18) shutter.

radiation above approximately 300 nm. Employing polychromatic radiation, the modeling here was based on the consideration that several different hypothetical monochromatic photoreactors could be assumed to work simultaneously, each one corresponding to a wavelength emitted by the lamp. The effects of all these hypothetically monochromatic reactors were then added to represent the polychromatic performance. Considering this particularity, the number of monochromatic hypothetical photoreactors differed between the two actual reactors, and in the case of Zalazar et al.,[28] absorption of titanium dioxide with the lamp used could extend to almost 260 nm, where radiation absorption by titanium dioxide is substantially larger. This produced a significant increase in the rate of electron−hole generation resulting from absorption of photons with much greater energy. This phenomenon, in turn, contributed to large values of the different primary quantum yields that were considered in an even enlarged set of wavelengths, which afterward, in the mathematical treatment, were averaged over the employed wavelength range (which, as said before, was very different between the two reactors). (7) Consequently, for a reactor working with an extended wavelength interval, particularly in the lower wavelength range, higher photoreactor efficiency would be expected in ref 28, because lower-wavelength radiation (with more energy) was available in the reaction space. In this sense, one should clearly note that truly effective intrinsic kinetics are comparable only when the lamps used and reactor windows are exactly the same, leading to the same spectral distribution and approximately the same order of magnitude, for each wavelength interval, of radiation arriving at the radiation-absorbing compound. (8) The study reported by Zalazar et al.[28] was focused on the effect of oxygen in the reaction, giving less emphasis to experiments with catalyst loading, whereas the objective of this work was mainly to investigate the influence of catalyst loading, and other parameters, on the degradation rate of DCA. (9) Finally, in this work, in accordance with the theoretical study conducted in Ballari et al.,[32,33] the reactor was always operated under conditions where the results could not be affected by external diffusive limitations at any time. All of these considerations generate an additional interest in this study because the obtained kinetics can be used to validate the models developed in Ballari et al.[32,33] concerning the mass-transfer limitations in slurry photocatalytic reactors.

This article begins by proposing the photocatalytic degradation mechanism of dichloroacetic acid. From this scheme, a kinetic reaction expression of DCA disappearance is developed in terms of parameters that affect the reaction rate, such as the local volumetric rate of photon absorption, the mass loading of titanium dioxide, the oxygen concentration (that will remain constant during this study), the DCA concentration, and the resistances existing in the catalytic primary particle agglomeration at low-pH conditions. Then, the results of the kinetic parameter estimation are shown, along with experimental data obtained from different experiments varying the operating conditions that affect the reaction rate. Finally, the estimated kinetic parameters are validated by comparison of the simulation data resulting from a perfectly mixed reactor model (according to the operating conditions defined in Ballari et al.[32,33]) with the experimental information obtained in the laboratory reactor.

2. Experimental Section

The experiments were carried out in a specially designed and built photoreactor that is part of a batch recirculation system. The apparatus was assembled with the following components (Figure 1 and Table 1): (i) one long parallelepiped (100 × 8 × 1 cm) made of stainless steel that includes, in a small part of its length (at its top), one flat-plate photoreactor resulting from the presence of one borosilicate glass window (15 × 8 cm) on each side of the parallelepiped; (ii) a stainless steel recirculating centrifugal pump (Simes Corp.) equipped with an electronic flow control; (iii) a calibrated rotameter; (iv) a well-stirred, 5000 cm^3 tank made of glass, isolated from the laboratory light, that included provisions for sampling and temperature measurements; (v) an oxygen bubbling system with a glass disperser, operating continuously in the tank to maintain a constant gas concentration in the reactor feed; (vi) a long, all-glass heat exchanger for temperature control connected to a thermostatic bath; and (vii) two lamps (one on each side of the windows) located horizontally at the focal axis of their respective custom-made parabolic reflectors, manufactured with specularly finished aluminum mirrors by the Alzak treatment from ALCOA. The radiation sources were medium-pressure mercury lamps (Philips HPA 1000) with a nominal input power of 1000 W each and polychromatic emission between 260 and 580 nm, with a well-known relative wavelength distribution of the output energy.

Table 1. Main Characteristics of the Experimental Setup

Reactor	
material	stainless steel
length	100 cm
width	8 cm
thickness	1 cm
total volume	800 cm^3
Photoreactor	
windows material	borosilicate glass
length	15 cm
entrance length	75 cm
width	8 cm
thickness	1 cm
volume	120 cm^3
Lamps	
model	Philips HPA 1000
number	2
input power	1000 W
length	8.5 cm
emission wavelength	260−580 nm
Parabolic Reflectors	
material	aluminum mirrors with Alzak treatment
aperture	20 cm
focal distance	2.78 cm
length	14 cm
Filters	
material	stainless steel mesh
attenuation	20% and 45%
Recirculating Pump	
material	stainless steel
operating power	0.5 HP
total maximum flow rate	182 $cm^3\ s^{-1}$
reactor maximum flow rate	76 $cm^3\ s^{-1}$
Pipes	
material	stainless steel
nominal diameter	0.95 cm
Tank	
material	glass
maximum volume	5000 cm^3
nominal total reactor volume	4000 cm^3

In addition, (viii) between each lamp system and the reactor window there was a fixed, flat borosilicate ground glass to produce diffuse emission toward the reaction space. (ix) It was also possible to interpose between the lamp and the reactor two additional devices: (1) a sliding shutter to determine exactly the moment at which the photocatalytic reaction started after the hydrodynamic and thermal steady state of the overall reaction system had been reached and (2) neutral density filters of different transmissions to change the intensity of the incident radiation on the reactor windows. (x) The operating temperatures of the lamps and reflectors were controlled with a variable-flow-rate air blower. (xi) An additional recirculation circuit for the tank alone was included to further improve mixing. (xii) The photoreactor, reflectors, and UV lamps were enclosed in a box to ensure safe operation, and (xiii) stainless steel tubing was used for all connections.

The employed reactants during the photocatalytic experiments were DCA (>98% purity, Merck), titanium dioxide (99.9% anastase, Aldrich), and oxygen (industrial-quality, >99.5% purity).

After the experimental device had been cleaned, the titanium dioxide suspension and DCA solution were loaded; the system flow rate and temperature were stabilized, with the latter kept at 20 °C; and extremely good mixing conditions were ensured. Oxygen was continuously fed into the tank to maintain a complete saturation concentration at all times. The lamps were turned on and stabilized for 20 min (while the shutters on the reactor windows were closed). Subsequently, the flow rate was controlled with the regulating valve, according to the rotameter measurements. Then, the sample at $t = 0$ min was taken at the same time that the lamp shutters were opened. Afterward, samples were taken every 30 min for several measurements. The total reaction time was 3 h for all experiments.

Table 2. Reaction Mechanism (from Reference 28)

reaction steps				no.	constant
TiO_2	$+ h\nu$	$\rightarrow h^+$	$+ e^-$	0	Φ_λ
$Site_{DCA}$	$+ CHCl_2COO^-$	$\leftrightarrow CHCl_2COO^-_{ads}$		1	K_1
$CHCl_2COO^-_{ads}$	$+ h^+$	$\rightarrow CHCl_2COO^\bullet$		2	k_2
$CHCl_2COO^\bullet$		$\rightarrow HCl_2C^\bullet$	$+ CO_2$	3	k_3
$Site_{O_2}$	$+ O_2$	$\leftrightarrow O_{2ads}$		4	K_4
O_{2ads}	$+ HCl_2C^\bullet$	$\rightarrow CHCl_2OO^\bullet$		5	k_5
$2CHCl_2OO^\bullet$		$\rightarrow 2COCl_2$	$+ H_2O_2$	6	k_6
$COCl_2$	$+ H_2O$	$\rightarrow CO_2$	$+ 2HCl$	7	k_7
h^+	$+ e^-$	$\rightarrow$ heat		8	k_8
O_{2ads}	$+ e^-$	$\rightarrow O_2^{\bullet-}$		9	k_9
$O_2^{\bullet-}$	$+ H^+$	$\rightarrow HO_2^\bullet$		10	k_{10}
$HO_2^\bullet$	$+ e^-$	$\rightarrow HO_2^-$		11	k_{11}
HO_2^-	$+ H^+$	$\rightarrow H_2O_2$		12	k_{12}

The concentrations of the reactants and products (DCA and chloride ion) of each sample were determined by ion-exchange chromatography (using 1.7×10^{-6} mol cm^{-3} CO_3HNa and 1.8×10^{-6} mol cm^{-3} CO_3Na_2 as the eluent, an IonPack AG4A-SC column, a Waters 432 conductivity detector, and an Alltech DS-Plus suppressor). In addition, a total organic carbon determination was performed with a TOC-5000A Shimadzu instrument, as a global measurement of the sample mineralization. Performing a carbon balance with the DCA concentration given by the chromatographic analysis and the TOC analysis, one can exclude the presence of stable organic intermediates if the two carbon balances agree, employing this indirect form of comparing information.

3. Reaction Scheme

The DCA photocatalytic mineralization mechanism was obtained from Zalazar et al.[28] (Table 2). This scheme considers that DCA, adsorbed on the catalyst surface, is attacked directly by a hole that is produced in the photocatalytic activation step, at acidic pH.[26,27,34] In actual terms, this model considers that, under acidic conditions, direct attack by holes is significantly more important than oxidation by $OH^\bullet$ radicals, a rather uncommon hypothesis compared to that more commonly employed in titanium photocatalysis, but clearly demonstrated in previous reports and reproduced in this contribution and in ref 28.

4. Kinetic Model

4.1. Degradation Kinetics of DCA. The rate of heterogeneous DCA decomposition can be precisely deduced by employing the following methodology and hypothesis: (1) Perform an active-site balance considering that DCA adsorption does not compete with oxygen adsorption.[35] (2) Relate the superficial concentration of DCA to the concentration in the bulk though an adsorption equilibrium constant. (3) Considering the very short lifetime and very small concentration of the unstable intermediates, in the unsteady-state reactor configuration, apply the microsteady-state approximation (MSSA). Then, according to the Appendix

$$R_{\mathrm{Het,DCA}} = \frac{k_2 C_{\mathrm{DCA_{ads}}} k_9 C_{\mathrm{O_{2ads}}} - \sqrt{(k_2 C_{\mathrm{DCA_{ads}}} k_9 C_{\mathrm{O_{2ads}}})^2 + 2 r_g k_9 C_{\mathrm{O_{2ads}}} k_2 C_{\mathrm{DCA_{ads}}} k_8}}{k_8} \quad (1)$$

The rate of the catalyst activation step for all wavelengths where titanium dioxide absorbs radiation can be expressed as a function of the local superficial rate of photon absorption (LSRPA)

$$r_g = \int_\lambda \Phi_\lambda e^a_{S,\lambda}\, d\lambda = \bar{\Phi}_\lambda \int_\lambda e^a_{S,\lambda}\, d\lambda \tag{2}$$

where

$$\bar{\Phi}_\lambda = \frac{\int_\lambda \Phi_\lambda e^a_{S,\lambda}\, d\lambda}{\int_\lambda e^a_{S,\lambda}\, d\lambda} \tag{3}$$

is the primary quantum yield averaged over all wavelengths where the photocatalyst absorbs radiation. This primary quantum yield does not include the recombination reaction of electrons and holes. This average was made because of the absence of detailed information concerning the value of the monochromatic quantum yield for each wavelength of the spectral range of radiation absorption by the catalyst. Rigorously speaking, this operation limits the validity of the model parameters to the spectral range of wavelengths emitted by the lamps that pass through the reactor walls and can be absorbed by the titanium oxide catalyst. Lamps with different wavelength emission distributions or power distributions at each wavelength, different reactor window materials, and different catalysts would result in a different value of $\bar{\Phi}_\lambda$. This is an unavoidable limitation unless radiation with equal monochromatic wavelength (with not-too-different output power), identical reactor wall materials, and the same catalyst are used. Thus, as an unfortunate consequence, in the majority of cases, even if the best and carefully selected operating conditions are employed, the results generally provide only pseudointrinsic kinetics.

Substituting the corresponding expressions for r_g (eq 2), the adsorbed DCA concentration (eq A.6 in the Appendix), and the adsorbed oxygen concentration (eq A.7 in the Appendix) into eq 1 and rearranging gives

$$R_{Het,DCA} = \frac{k_2 k_9 C_{sites O_2,T} K_4 C_{O_2} C_{sites DCA,T} K_1 C_{DCA}}{k_8 (1 + K_1 C_{DCA})(1 + K_4 C_{O_2})} \times \left[1 - \sqrt{1 + 2\bar{\Phi}_\lambda \int_\lambda e^a_{S,\lambda}\, d\lambda \, \frac{k_8 (1 + K_1 C_{DCA})(1 + K_4 C_{O_2})}{k_2 k_9 C_{sites O_2,T} K_4 C_{O_2} C_{sites DCA,T} K_1 C_{DCA}}}\right] \tag{4}$$

Lumping all possible kinetic constants and considering that the oxygen concentration remains constant during the reaction (because pure oxygen is continuously supplied to the system), the resulting expression for the superficial rate of dichloroacetic acid degradation is

$$R_{Het,DCA} = \frac{\alpha_1 C_{DCA}}{(1 + K_1 C_{DCA})}\left(1 - \sqrt{1 + 2\alpha_2 \int_\lambda e^a_{S,\lambda}\, d\lambda \, \frac{1 + K_1 C_{DCA}}{C_{DCA}}}\right) \tag{5}$$

where

$$\alpha_1 = \frac{k_2 k_9 C_{sites O_2,T} K_4 C_{O_2} C_{sites DCA,T} K_1}{k_8 (1 + K_4 C_{O_2})} \tag{6}$$

and

$$\alpha_2 = \frac{\bar{\Phi}_\lambda k_8 (1 + K_4 C_{O_2})}{k_2 k_9 C_{sites O_2,T} K_4 C_{O_2} C_{sites DCA,T} K_1} \tag{7}$$

4.2. DCA Degradation Rate per Unit Volume of Suspension. Once an expression for the DCA superficial reaction rate has been obtained, the result has to be brought from the catalytic surface to the suspension volume (where the measurements are made). The reaction rate per unit catalytic area is affected by the TiO_2 interfacial area per unit suspension volume, a_v. The pseudohomogeneous reaction rate expression per unit suspension volume is

$$R_{DCA} = R_{Het,DCA} a_V = C_{mc} S_g \frac{\alpha_1 C_{DCA}}{(1 + K_1 C_{DCA})}\left(1 - \sqrt{1 + 2\alpha_2 \int_\lambda e^a_{S,\lambda}\, d\lambda \, \frac{1 + K_1 C_{DCA}}{C_{DCA}}}\right) \tag{8}$$

with

$$a_V = C_{mc} S_g \tag{9}$$

where C_{mc} is the catalyst loading and S_g is the specific surface area of titanium dioxide.

Likewise, the local superficial rate of photon absorption (LSRPA) can be transformed into a local volumetric rate of photon absorption (LVRPA) according to

$$R_{DCA} = R_{Het,DCA} a_V = C_{mc} S_g \frac{\alpha_1 C_{DCA}}{(1 + K_1 C_{DCA})}\left[1 - \sqrt{1 + \frac{2\alpha_2 \int_\lambda e^a_\lambda\, d\lambda \, (1 + K_1 C_{DCA})}{C_{mc} S_g C_{DCA}}}\right] \tag{10}$$

4.3. Limiting Cases of the Kinetic Expression for DCA Degradation. For low DCA concentrations within the bulk of the fluid, the concentrations of adsorbed species are linearly proportional to the suspension concentration. Therefore, the DCA reaction rate is

$$R_{DCA} = C_{mc} S_g \alpha_1 C_{DCA}\left(1 - \sqrt{1 + \frac{2\alpha_2 \int_\lambda e^a_\lambda\, d\lambda}{C_{mc} S_g C_{DCA}}}\right) \tag{11}$$

This approach is valid for this kind of study, where contaminant species are present at low concentrations. In the same way, it can be safely applied to oxygen, because oxygen has a low water saturation limit. In addition, the value of K_1 in eq 10 is much less than 1, thereby making $K_1 C_{DCA} \ll 1$, as shown below.

When the reactor is subjected to medium to high rates of photon absorption, the term that contains the LVRPA is significantly higher than the others, and the reaction rate can be approximated by

$$R_{DCA} = -\alpha_1 \sqrt{2\alpha_2 \int_\lambda e^a_\lambda\, d\lambda \; C_{mc} S_g C_{DCA}} \tag{12}$$

In this way, a square-root dependence of the pollutant reaction rate on the LVRPA is obtained, as predicted in Alfano et al.[36] for high irradiation levels.

On the other hand, the square root in eq 11 can be analyzed in terms of a Taylor series expansion, resulting in a simplification that renders a second limiting case.[36] Therefore, when the irradiation rate is low, a linear dependence of the reaction rate on the LVRPA is obtained

$$R_{DCA} = \alpha_2 \alpha_1 \int_\lambda e^a_\lambda\, d\lambda \tag{13}$$

This result has been reported frequently in the photocatalytic literature, particularly for irradiation rates on the order of one sun or less.[37,38]

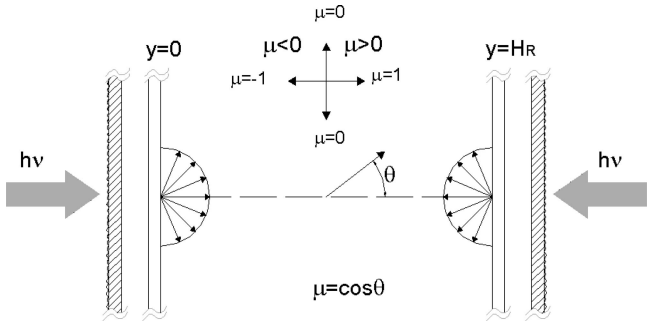

Figure 2. Schematic representation of the radiation field inside the reactor.

5. Radiation Balance

The presence of the term e_λ^a makes necessary to resort to the solution of the radiative transfer equation (RTE) in a participating medium, with absorption and scattering (no emission is considered because AOT reactions are normally carried out at ambient temperature)[39,40]

$$\frac{dI_{\lambda,\underline{\Omega}}(s,t)}{ds}+\kappa_\lambda(s,t)\,I_{\lambda,\underline{\Omega}}(s,t)+\sigma_\lambda(s,t)\,I_{\lambda,\underline{\Omega}}(s,t)=\frac{\sigma_\lambda(s,t)}{4\pi}\int_{\Omega'=4\pi}p(\Omega'\rightarrow\Omega)\,I_{\lambda,\overline{\Omega}'}(s,t)\,d\Omega' \quad (14)$$

where the second and third terms on the left-hand side represent absorption and outscattering, respectively, and the right-hand side represents inscattering.

For the case of a one-dimensional slab geometry (Figure 2) with azimuthal symmetry resulting from the diffuse irradiation of the reactor windows, as a consequence of the employed ground glass device, the RTE becomes the one-dimensional−one-directional radiation model[41]

$$\mu\frac{dI_\lambda(y,\mu)}{dy}+(\kappa_\lambda+\sigma_\lambda)I_\lambda(y,\mu)=\frac{\sigma_\lambda}{2}\int_{\mu'=-1}^{\mu'=1}I_\lambda(y,\mu')\,p(\mu,\mu')\,d\mu' \quad (15)$$

Note that $\kappa_\lambda + \sigma_\lambda = \beta_\lambda$, the extinction coefficient, and $\mu = \cos\theta$.

The diffuse and isotropic inlet boundary conditions are

$$I_\lambda(y=0,\mu)=I_\lambda^0 \qquad \text{for } \mu>0 \quad (16)$$

$$I_\lambda(y=H_R,\mu)=I_\lambda^{H_R} \qquad \text{for } \mu<0 \quad (17)$$

In accordance with Satuf et al.,[29] the Henyey and Greenstein (HG) phase function was used[42,43]

$$p_{HG,\lambda}(\mu_0)=\frac{1-g_\lambda^{\,2}}{(1+g_\lambda^{\,2}-2g_\lambda\mu_0)^{3/2}} \quad (18)$$

where μ_0 is the cosine of the angle between the direction of propagation of the incoming scattered ray and that for which the RTE is written.

The solution of eqs 15−18 was numerically obtained with the discrete ordinate method.[44] From the values of the specific intensities, the local volumetric rate of photon absorption (LVRPA) for the one-dimensional−one-directional radiation model is obtained as

$$e_\lambda^a[(y),C_{mc}]=\kappa_\lambda\left\{2\pi\int_{\mu=-1}^{\mu=1}I_\lambda[(y,\mu),C_{mc}]\,d\mu\right\} \quad (19)$$

5.1. Optical Properties. The catalyst used in this study was obtained from Aldrich (>99.9% anatase). The values of the dimensionless asymmetry factor, g_λ, and other optical properties for the employed catalyst for acid suspensions (pH 2.5), as determined by Satuf et al.,[30] are listed in Table 3. Also included in this table are the spectral emission energy distribution of the lamp, f_λ, and the borosilicate glass transmittance, T_λ, for the useful range of employed wavelengths (considering absorption by TiO_2 and transmission by the borosilicate glass windows).

5.2. Determination of the Boundary Condition for the RTE. The values of the total radiative flux, $q_{W,T}$ (275 nm ≤ λ ≤ 390 nm), on each side of the reactor windows, with and without filters, were measured by potassium ferrioxalate actinometry[45] and are reported in Table 4. These values were calculated according to the approach of Zalazar et al.[46] and Brandi et al.[47] Starting from the mass balance for Fe^{2+}

$$\frac{dC_{Fe^{2+},Tk}(t)}{dt}=\frac{V_R}{V_T}\sum_\lambda\langle R_{Act,\lambda}(y,t)\rangle_{A_{S,R}} \quad (20)$$

and considering that the reaction rate for the actinometer is

$$\sum_\lambda\langle R_{Act,\lambda}(y,t)\rangle_{A_{S,R}}=\sum_\lambda\Phi_{Act,\lambda}\langle e^a_{Act,\lambda}(y,t)\rangle_{A_{S,R}} \quad (21)$$

and the RTE for the homogeneous medium is

$$\mu\frac{dI_{\lambda,\underline{\Omega}}(y,t)}{dy}+\kappa_{T,\lambda}(t)I_{\lambda,\underline{\Omega}}(y,t)=0 \quad (22)$$

the resulting total radiative flux on each side of the reactor, obtained after solving eqs 20−22, is

$$q_{W,T}=\frac{V_T H_R}{V_R}\left[\lim_{t\rightarrow0}\frac{dC_{Fe^{2+},Tk}}{dt}\right]\times\frac{1}{\sum_\lambda\Phi_{Act,\lambda}f_\lambda T_\lambda\{1-2E_3[\kappa_{Fe^{3+},\lambda}(t\rightarrow0)H_R]\}} \quad (23)$$

where $\lim_{t\rightarrow0}(dC_{Fe^{2+},Tk}/dt)$ is given by the experimental data of the initial generation rate of Fe^{2+}, $\Phi_{Act,\lambda}$ is the overall quantum yield for the actinometer,[45] $\kappa_{Fe^{3+},\lambda}=\alpha_{Fe^{3+},\lambda}C_{Fe^{3+}}$ is the absorption coefficient of Fe^{3+} solution, being $\alpha_{Fe^{3+},\lambda}$ the molar Naperian absorptivity of Fe^{3+},[45] and E_3 is the third-order integral exponential function.[39,42] Equation 23 takes into account the fact that, even though titanium dioxide absorbs radiation up to 385−390 nm, the actinometer solution absorbs photons much beyond this limit, but with a small absorption coefficient. Consequently, the more simplified equation that is very often used is not applicable in this case. For more details, see Zalazar et al.[46]

From the total radiation flux values, the boundary condition of the RTE can be calculated as

$$I_\lambda^0=\frac{q_{W,T}f_\lambda T_\lambda}{\pi} \quad (24)$$

6. Mass Balance

A limiting operation of the system could be achieved if the reactor were operated with differential conversion and/or if the reactor volume were much smaller than the total reaction volume($V_R/V_T \ll 1$) and the tank and reactor were extremely well mixed. These conditions were achieved in the experimental device considering the analysis made in Ballari et al.,[32] where the mass-transfer limitations and the operating conditions that contribute to their emergence were studied. Thus, the perfect mixed model (PMM) could be applied for the mass balance in the reactor. However, the experiments were performed at acidic pH, which favors the formation of agglomerates. Consequently, it was neces-

Table 3. Spectral Distribution of Catalyst Optical Properties (pH 2.5),[a] Relative Emission of the Lamp, and Borosilicate Glass Transmittance

wavelength (nm)	β^*_γ(cm^2 g^{-1})	β^*_κ(cm^2 g^{-1})	g_λ ($-1 \le g_\lambda \le 1$)	f_λ (E_λ/E_T)	$T_\lambda \times 100$ (%)
275	14071.0	5606.0	0.8768	0.0104	0.05
305	14167.0	5703.4	0.8973	0.0431	36.55
310	14182.5	5725.3	0.90175	0.0526	48.80
324	14324.9	5759.62	0.89486	0.033	73.33
359	15016.2	3731.12	0.65954	0.085	90.00
370	15145.0	1051.84	0.54235	0.139	90.00
385	15249.0	758.38	0.4759	0.104	90.00

[a] Aldrich titanium dioxide. $S_g = 9.6$ m^2 g^{-1}, nominal size of the primary particle = 200 nm.

Table 4. Actinometry Results

actinometry	irradiation level (%)	$\lim_{t\to 0}(dC_{Fe^{2+},Tk}/dt) \times 10^8$ (mol cm^{-3} s^{-1})	$q_{W,T} \times 10^6$ (Einstein cm^{-2} s^{-1})
right lamp without filter	100.0	1.27	1.13
left lamp without filter	100.0	1.24	1.11
right lamp with low attenuation filter	45.55	0.58	0.52
left lamp with low attenuation filter	44.97	0.56	0.50
right lamp with high attenuation filter	19.16	0.24	0.22
left lamp with high attenuation filter	19.90	0.25	0.22

sary to implement an overall effectiveness factor in the mass balance, as discussed by Ballari et al.,[25] in order to consider the internal mass and radiation resistances inside the catalyst. Therefore, the mass balance of DCA (A) for a perfect mixed reactor is

$$\frac{dC_{A,Tk}(t)}{dt} = \frac{V_R}{V_T} a_V \langle R_{Het,A}(r,y,t)\rangle_{A_{S,R}} = \frac{V_R}{V_T} a_V \eta_0 \langle R_{Het,A}(R_P,y,t)\rangle_{A_{S,R}} \tag{25}$$

with

$$C_{A,Tk}(t=0) = C_A^0 \tag{26}$$

and

$$\begin{aligned}\eta_0 &= \frac{\langle R_{V_P,A}[C_A(r), e^a_S(r)]\rangle_{V_P}}{R_{V_P,A}[C^s_A(R_P), e^a_S(R_P)]} \\ &= \frac{\langle R_{V_P,A}[C_A(r), e^a_S(r)]\rangle_{V_P}}{\langle R_{V_P,A}[C^s_A(R_P), e^a_S(r)]\rangle_{V_P}} \times \frac{\langle R_{V_P,A}[C^s_A(R_P), e^a_S(r)]\rangle_{V_P}}{R_{V_P,A}[C^s_A(R_P), e^a_S(R_P)]} \\ &= \eta_{Diff} \times \eta_{Att}\end{aligned} \tag{27}$$

where $R_{V_P,A} = a_{V_P} R_{Het,A}$ is the DCA reaction rate per unit particle or agglomerate volume, with $a_{V_P} = S_g \rho_S (1 - \varepsilon_P)$ being the solid−liquid interfacial area per unit particle volume. In the second line of eq 27, the two terms represent the diffusive mass-transfer effectiveness factor (η_{Diff}) and the photon transport effectiveness factor (η_{Att}), respectively. The effectiveness factors can be calculated solving the mass balance inside an assumed spherical shape for the solid agglomerate.[25] Additionally, the local superficial rate of photon absorption inside the porous agglomeration of primary particles can be calculated, according to Ballari et al.,[25] from

$$e^a_S(r) = \frac{e^a_\lambda[(y), C_{mc}]}{S_g C_{mc}} \frac{R_P}{r} \frac{\sinh(\gamma r)}{\sinh(\gamma R_P)} \frac{1}{\frac{3}{\gamma R_P}\left[\frac{1}{\tanh(\gamma R_P)} - \frac{1}{\gamma R_P}\right]} \tag{28}$$

with $\gamma^2 = 3(1 - \omega_P)\,\beta_P^2$.

In this way, introducing the effectiveness factor, a mass balance equation was obtained that depends on the bulk properties, independently of what happens inside the agglomerated particle. The result is valid if there are no external mass-transfer resistances in the outside film of the particle, as was demonstrated by Ballari et al.[25] for the particle and agglomerate sizes typically used in photocatalysis with titanium dioxide suspensions.

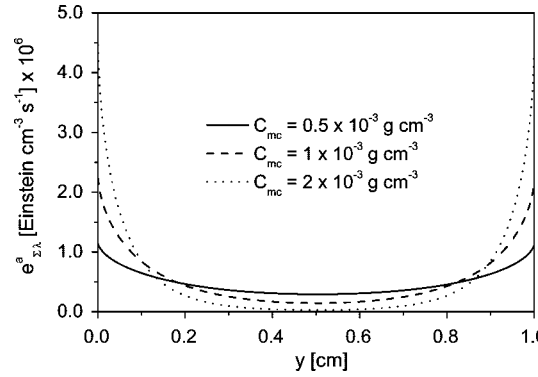

Figure 3. Local volumetric rate of photon absorption as a function of the main characteristic dimension for radiation propagation inside the reactor space.

7. Results

7.1. Radiation Profiles in the Reactor. Figure 3 shows the LVRPA profiles ($e^a_{\Sigma\lambda}$) inside the reactor as a function of the reactor thickness (y) for several catalyst loadings that were employed in different experiments and for a value corresponding to 100% of the incident radiation (Table 4). These LVRPA profiles were obtained by employing catalyst optical properties at acidic pH. The observed radiation attenuation is significantly smaller when these profiles are compared with those obtained at natural pH. This is consistent with experiments showing that the extinction coefficient at acidic pH[30] is lower than at neutral pH.[29]

7.2. Photocatalytic Experiments. Prior to the execution of the photocatalytic experiments, the DCA adsorption on the overall system was verified by performing a dark run (UV lamps off) with $C_{mc} = 1 \times 10^{-3}$ g cm^{-3}. The DCA concentration remained invariant over time ($t = 0$ min, $C_A = 1.00 \times 10^{-6}$ mol cm^{-3}; $t = 60$ min, $C_A = 1.02 \times 10^{-6}$ mol cm^{-3}; $t = 120$ min, $C_A = 0.99 \times 10^{-6}$ mol cm^{-3}), which could dismiss the occurrence of DCA adsorption on the different materials that form part of the experimental device.

Different experimental runs were performed in the laboratory varying the main parameters that influence the photocatalytic reaction, as shown in Table 5. These parameters are the catalyst mass loading, initial contaminant concentration, and incident irradiation level. In all these experiments, the maximum operating flow rate was used, because it was intended to work without concentration gradients in the reactor. Thus, it was possible to obtain good mixing conditions in the reactor, and according to the choice of the rest of the operating variables analyzed in Ballari et al.,[32] an intrinsic kinetic model of

Table 5. Photocatalytic Experiments

experiment	$C_{mc} \times 10^3$ (g cm^{-3})	$C_A^0 \times 10^6$ (mol cm^{-3})	irradiation level (%)	experimental conversion (%)	model conversion (%)	error (%)
1	0.1	1	100	38.04	34.06	4.37
2	0.1	1	45	26.81	29.16	2.06
3	0.1	0.5	100	45.46	49.83	4.78
4	0.25	1	100	50.44	58.27	8.79
5	0.25	1	45	55.83	49.74	7.18
6	0.25	1	20	34.57	31.47	2.78
7	0.25	0.5	100	70.75	75.01	6.43
8	0.5	1	100	77.48	79.80	3.96
9	0.5	1	45	68.31	70.39	4.25
10	0.5	1	20	43.07	44.84	3.17
11	0.5	0.5	100	92.86	94.44	14.23
12	1	1	45	85.19	86.53	6.18
13	1	1	20	57.88	58.10	1.07
14	2	1	20	65.87	67.74	2.59

dichloroacetic acid degradation observed over the catalytic surface could be determined. In other words, these kinetic parameters were obtained under conditions that were free of mass-transfer limitations.

In Figure 4, some of these experimental results are shown in terms of DCA, equivalent stoichiometric chloride, and equivalent TOC concentrations; i.e., all of these determinations are expressed as DCA concentrations. Good agreement between the three concentrations can be observed. It can be seen that DCA degradation does not produce stable organic intermediates, because the DCA concentration chromatographically determined, is almost equal to the DCA concentration in terms of equivalent TOC measurements. In addition, it can be concluded that the reaction stoichiometry was satisfied, because 1 mol of DCA generated 2 mol of chloride.

7.3. Estimation of Kinetic Parameters. To estimate the kinetic parameters, the modified Levenberg−Marquardt method was employed. This is an algorithm to optimize the estimation

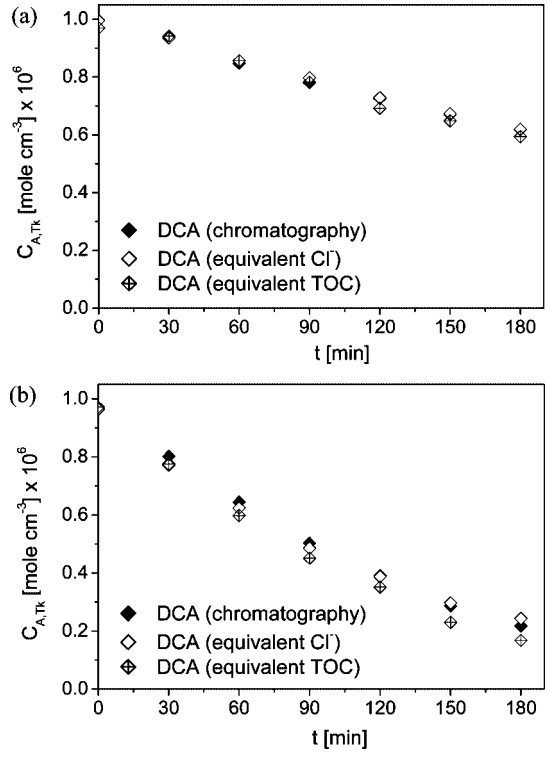

Figure 4. Experimental results of tank DCA concentration evolution. (a) Experiment 1: $C_{mc} = 0.1 \times 10^{-3}$ g cm^{-3}, $C_A^0 = 1 \times 10^{-6}$ mol cm^{-3}, irradiation level = 100%. (b) Experiment 8: $C_{mc} = 0.5 \times 10^{-3}$ g cm^{-3}, $C_A^0 = 1 \times 10^{-6}$ mol cm^{-3}, irradiation level = 100%.

of nonlinear multiparameter expressions, by comparing predictions from theoretical models with experimental data and minimizing the sum of the square of the error differences.

The kinetic equation used for parameter optimization was eq 11, which considers a linear adsorption rate of oxygen and DCA. Previously, the validity of this hypothesis (the linear adsorption rate) was demonstrated using eq 10 for the parameter estimation. In this estimation, a value of K_1 much less than unity was obtained ($K_1 < 10^{-6}$ cm^3 mol^{-1}).

In addition, it was considered that the effectiveness factor remained constant for the employed reactor operating conditions. However, its value was different from 1.0. As shown in Ballari et al.,[25] the overall effectiveness factor differs significantly from 1.0 because of the contribution of the photon transport effectiveness factor in the catalytic agglomerate. This hypothesis can be validated by calculating the polychromatic effectiveness factor according to Ballari et al.[25] and eq 27. To this end, the optimized kinetic parameters for the most extreme operating conditions of the system must be used: (i) catalyst loading (0.1 and 2 g L^{-1}), (ii) irradiation level (on the wall and at the reactor center), and (iii) pollutant concentration (at the initial and final reaction times, t_0 and t_F, respectively). For an average agglomerate size of 2.5 μm (determined by optical microscopy for a suspension at pH 3), the average value of the effectiveness factor with its corresponding standard deviation was found to be

$$\eta_0 = 0.324 \pm 0.014 \tag{29}$$

Observing the standard deviation, which does not exceed 5% of the average value, a constant effectiveness factor for the experimental conditions employed can be justified.

Summarizing, the ordinary differential equation employed for the parameter estimation, considering eqs 11 and 25, was

$$\frac{dC_{A,Tk}(t)}{dt} = \frac{V_R}{V_T} C_{mc} S_g \eta_0 \alpha_1 C_{A,Tk}(t) \times \left\langle \left\{ 1 - \sqrt{1 + \frac{2\alpha_2 \int_{\lambda=275\text{ nm}}^{\lambda=390\text{ nm}} e_\lambda^a[(y), C_{mc}]\, d\lambda}{C_{mc} S_g C_{A,Tk}(t)}} \right\} \right\rangle_{A_{S,R}} \tag{30}$$

with the initial condition

$$C_{A,Tk}(t=0) = C_A^0 \tag{31}$$

The kinetic parameters estimated with the Levenberg−Marquardt method and their corresponding 95% confidence intervals were obtained as

$$\alpha_1 = (38.89 \pm 2.14) \times 10^{-7} \text{ cm s}^{-1} \tag{32}$$

$$\alpha_2 = (1.64 \pm 0.35) \times 10^5 \text{ mol s Einstein}^{-1} \text{ cm}^{-1} \quad (33)$$

With the estimated kinetic parameters (eqs 32 and 33), the primary quantum yield of the photocatalytic reaction, averaged over the employed wavelength range, was calculated as

$$\bar{\Phi}_\lambda = \alpha_1 \alpha_2 = 0.637 \pm 0.171 \text{ mol Einstein}^{-1} \quad (34)$$

This value of the quantum yield is between 0 and 1, which is a good indication that the parameter estimation is providing a value that under no circumstances contradicts the physical interpretation of the activation step.

7.4. Experimental Results versus Model. To show the ability of the model to represent the full set of data, with the previously determined kinetic parameters, different experiments were simulated with the complete computer program. Then, the DCA concentration data from the laboratory and those from the model, both as a function of time, were compared. The model shows good agreement with all of the experimental results, with a total root-mean-square error defined as

$$\text{error (\%)} = \sqrt{\frac{\sum_{i=1}^{N} \left(\frac{C^i_{\text{A,Experimental}} - C^i_{\text{A,Model}}}{C^i_{\text{A,Experimental}}} \times 100 \right)^2}{N}} \quad (35)$$

equal to 6.07%.

This error is shown for each experiment in Table 5. The maximum deviation in some particular cases never exceeded 15%. In addition, the total experimental and model calculated conversions for an experimental time of 3 h ($t_F = 180$ min) are reported in Table 5 for each experiment.

Figures 5−7 show the results calculated with the perfect mixed model (which was used to estimate the parameters) and the experimental data on DCA concentration measured in the tank by ion-exchange chromatography for each experiment. In all cases, the agreement of the results is more than acceptable.

It is possible to analyze the effects of different operating variables on the system by resorting to the estimated kinetic parameters. This analysis can include a comparison between simulated values obtained with the model and experimental measurements.

It can be observed that, for the same irradiation rate and the same initial DCA concentration, when the reactor operates under perfect mixing conditions and there are no mass-transfer limitations in the bulk of the fluid, increasing the catalyst loading results in an increase in the final conversion. Figure 5a−d shows, for different irradiation rates and different initial DCA concentrations, the results produced by changing the catalyst loading. Both the experimental values and model simulations indicate that conversion always increases when the loading of titanium dioxide increases. It should be noted that this result is valid only for the case of the assumed perfect mixing conditions. This result was also reported in a theoretical study by Ballari et al.[32]

Figure 6 compares different runs made with varying initial DCA concentration, a mass catalyst loading equal to 0.5×10^{-3} g cm^{-3}, and 100% of the available irradiation rate. As expected, decreasing the concentration of the pollutant increases the final conversion of the reaction system.

For a given catalyst loading and a fixed initial pollutant concentration, when the irradiation level produced by the lamps is reduced, the final conversion also decreases (Figure 7). In a first approximation, it could be said that the plot looks like a square-root dependence. However, even if this observation were, to some extent, partially true, in reality, what is depicted in the curve is a mixed dependence with a preponderant influence of a form close to a square-root function. What is quite clear is that a neat linear behavior is far from being achieved. As a way of illustration, it can be seen that, when the irradiation level is reduced to 45% of the maximum value, the final conversion does not change in the same proportion; on the contrary, it is notably larger. This is a direct result of the radiation power of the employed lamp. Linear dependences are clearly noticed only at very low irradiation rates.

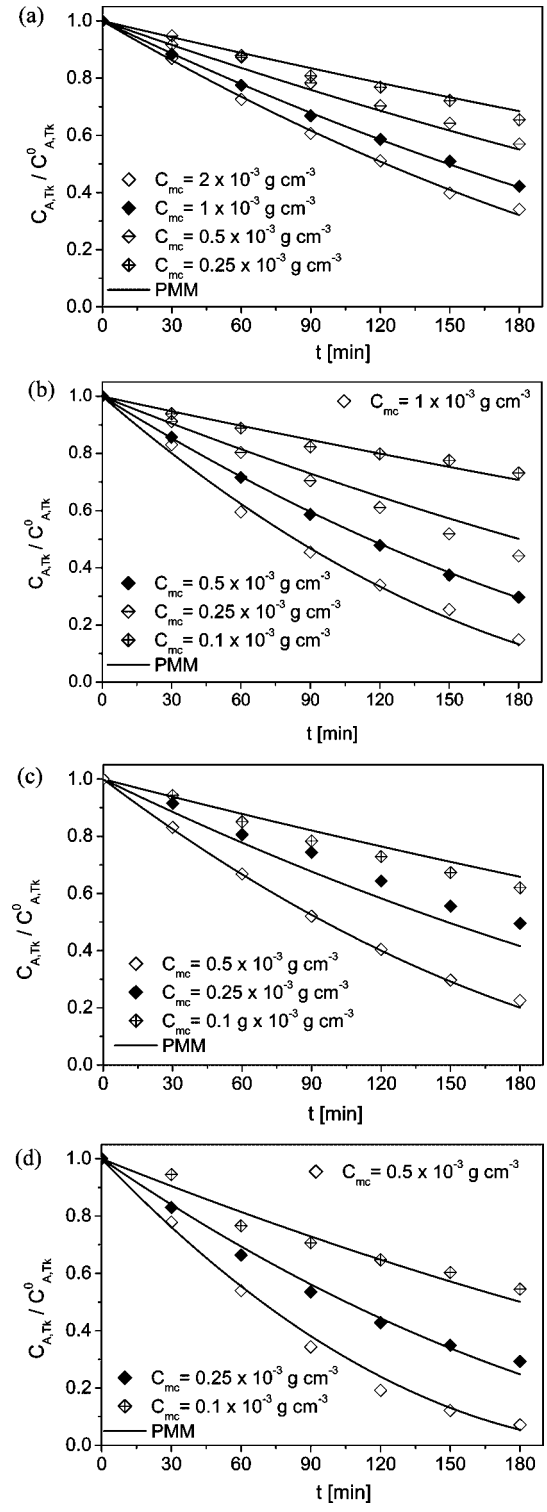

Figure 5. Tank DCA concentration evolution for different catalyst loadings. (a) $C^0_A = 1 \times 10^{-6}$ mol cm^{-3}, irradiation level = 20%. (b) $C^0_A = 1 \times 10^{-6}$ mol cm^{-3}, irradiation level = 45%. (c) $C^0_A = 1 \times 10^{-6}$ mol cm^{-3}, irradiation level = 100%. (d) $C^0_A = 0.5 \times 10^{-6}$ mol cm^{-3}, irradiation level = 100%.

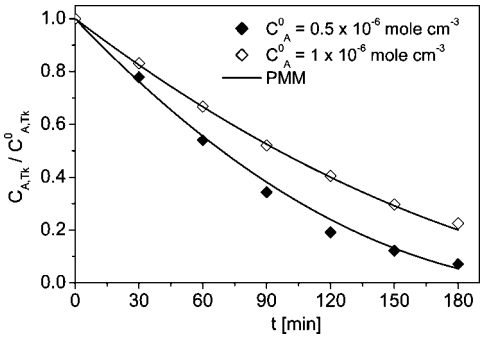

Figure 6. Tank DCA concentration evolution for different initial contaminant concentrations. $C_{mc} = 0.5 \times 10^{-3}$ g cm^{-3}, irradiation level = 100%.

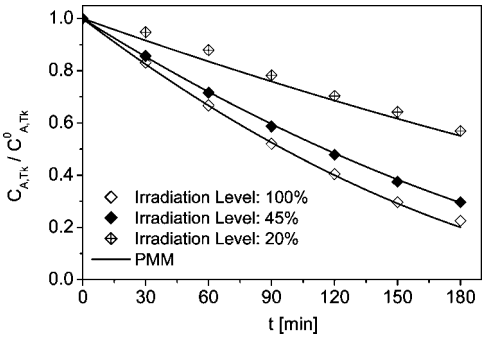

Figure 7. Tank DCA concentration evolution for different irradiation levels. $C_{mc} = 0.5 \times 10^{-3}$ g cm^{-3}, $C^0_A = 1$ mM.

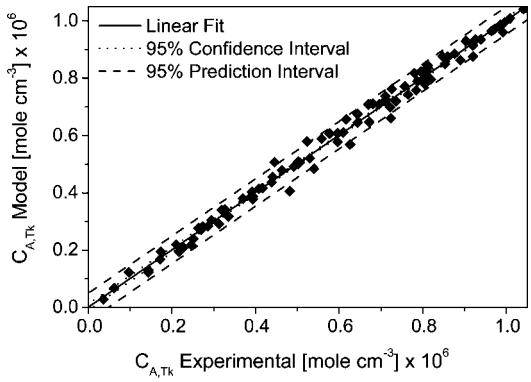

Figure 8. DCA concentration simulated by the model employing the estimated kinetic parameters versus experimental DCA concentration. Linear regression with the corresponding predicted and confidence intervals.

Table 6. Linear Regression Results of the DCA Concentration Model versus the Experimental Data

			95% confidence interval	
parameter	value	error	lower limit	upper limit
slope	1.00116	0.00893	0.98344	1.01888
ordinate intercept	0.00091	0.00594	−0.01088	0.0127
R^2	0.99243			
N^a	98			

[a] Number of data points.

The predicted DCA concentrations were then plotted against the DCA experimental concentration in the tank. The linear regression of these values should give a line with a slope close to 1 and an ordinate intercept equal to 0. These results are shown in Figure 8 and Table 6.

Another way to demonstrate that the parameter estimation is satisfactory and, at the same time, to validate the kinetic, radiation, and reactor models and the estimation of the photocatalytic effectiveness factor is to employ the obtained kinetic constants in a more complete model. This must be done under different operating conditions outside the kinetic controlling regime (e.g., for other catalyst loadings, irradiation rates, and volumetric flow rates). This verification will be made in a forthcoming work, using the models developed by Ballari et al.[32,33]

8. Conclusions

In this work, a kinetic study of the photocatalytic degradation of dichloroacetic acid (DCA) was conducted. This analysis involved a proposed photocatalytic reaction mechanism and the development of a heterogeneous kinetic expression for the disappearance of the pollutant. Several experiments were carried out in the laboratory with the system under very good mixing conditions. With these experimental data and the kinetic expression, the kinetic parameters were estimated using a perfect mixed model for the mass balance and a one-dimensional−one-directional radiation model to calculate the photon absorption rate. This mass balance was affected by an effectiveness factor considering mass and photon-transfer restrictions inside the primary particle agglomeration of titanium dioxide. This restriction is mainly due to radiation-transfer limitations. For the operating conditions used in this study, it was shown that the effectiveness factor is low and remains nearly constant along the reaction. Employing the estimated kinetic parameters, a very good correlation between the experimental data and the computer simulation with the theoretical model was obtained, with a total root-mean-square error equal to 6.07%.

Acknowledgment

Thanks are given to Universidad Nacional del Litoral, CONICET, and Agencia Nacional de Promoción Científica y Tecnológica for financial help. M.M.B. acknowledges CONICET for the awarded doctoral fellowship.

Nomenclature

A = area (cm^2)
a_V = solid−liquid interfacial area per unit reactor volume (cm^2 cm^{-3})
a_{V_P} = solid−liquid interfacial area per unit particle volume (cm^2 cm^{-3})
C_i = molar concentration of generic component i (mol cm^{-3})
$C_{i_{ads}}$ = superficial concentration of generic component i (mol cm^{-2})
C_{h^+} = superficial concentration of holes or vacancies (mol cm^{-2})
C_{e^-} = superficial concentration of electrons (mol cm^{-2})
C_{sites} = superficial concentration of active sites (mol cm^{-2})
C_{mc} = catalyst mass loading (g cm^{-3})
e^a = local volumetric rate of photon absorption (Einstein s^{-1} cm^{-3})
e^a_S = local superficial rate of photon absorption (Einstein s^{-1} cm^{-2})
E = radiant energy (Einstein)
E_n = integral exponential function of order n (dimensionless)
f = spectral emission energy distribution of the lamp (dimensionless)
g = parameter in the phase function for scattering (dimensionless)
H = reactor depth (cm)
I = specific radiation intensity (Einstein s^{-1} cm^{-2} sr^{-1})
k = kinetic constant; units depend on the reaction step
K = equilibrium constant (cm^3 mol^{-1})
p = phase function (dimensionless)
q = radiative flux (Einstein s^{-1} cm^{-2})
r = radial coordinate (cm) or elemental superficial reaction rate (mol s^{-1} cm^{-2})

R = radius (cm) or pseudohomogeneous reaction rate (mol s^{-1} cm^{-3})
R_{Het} = heterogeneous reaction rate (mol s^{-1} cm^{-2})
R_{V_P} = reaction rate per unit particle volume (mol s^{-1} cm^{-3})
s = spatial coordinate along a given direction of radiation propagation (cm)
S_g = specific catalyst surface area (cm^2 g^{-1})
t = time (s)
T = transmittance (dimensionless)
V = volume (cm^3)
y = Cartesian coordinate (cm)

Greek Letters

α = molar Naperian absorptivity (cm^2 mol^{-1})
α_1 = kinetic parameter (cm s^{-1})
α_2 = kinetic parameter (mol s $Einstein^{-1}$ cm^{-1})
β = volumetric extinction coefficient (cm^{-1})
ε_p = porosity (dimensionless)
η = effectiveness factor (dimensionless)
Φ = quantum yield (mol $Einstein^{-1}$)
κ = volumetric absorption coefficient (cm^{-1})
λ = wavelength (nm)
μ = cos θ (dimensionless)
μ_0 = cosine of the angle between an incoming and a scattered ray (dimensionless)
θ = spherical coordinate (rad)
ρ = density (g cm^{-3})
σ = volumetric scattering coefficient (cm^{-1})
$\omega = \sigma/\beta$ = albedo (dimensionless)
Ω = solid angle (sr)
$\underline{\Omega}$ = unit vector in the direction of radiation propagation (dimensionless)

Subscripts

0 = global
ads = adsorption
A = dichloroacetic acid (DCA)
Act = actinometer
c = catalyst
F = final
P = particle or agglomerate
R = reactor
S = solid or superficial variable
sites = active sites
T = total
Tk = tank
W = wall of the reactor
λ = wavelength
Ω = direction of radiation propagation

Superscripts

* = specific properties
0 = initial value or at $y = 0$
H_R = surface at $y = H_R$

Special Symbols

$\langle\rangle$ = average value over a defined space
$\overline{\ }$ = average value over wavelengths

Appendix

A.1. Balance of Active Sites

The superficial rate corresponding to the adsorption and desorption step of DCA on the superficial active sites of catalyst can be expressed as

$$r_1 = k_{1+} C_{sitesDCA} C_{DCA} - k_{1-} C_{DCA_{ads}} \quad (A.1)$$

In equilibrium, the superficial concentration of adsorbed DCA is related to the DCA concentration in the bulk of the fluid through the adsorption equilibrium constant

$$C_{DCA_{ads}} = K_1 C_{sitesDCA} C_{DCA} \quad (A.2)$$

A balance of vacant sites for DCA adsorption, total sites, and occupied sites gives

$$C_{sitesDCA,T} = C_{sitesDCA} + C_{DCA_{ads}} \quad (A.3)$$

Substituting the adsorbed DCA concentration given by eq A.2 into eq A.3 gives

$$C_{sitesDCA,T} = C_{sitesDCA} + K_1 C_{sitesDCA} C_{DCA} \quad (A.4)$$

Solving for the concentration of sites available for DCA adsorption yields

$$C_{sitesDCA} = \frac{C_{sitesDCA,T}}{1 + K_1 C_{DCA}} \quad (A.5)$$

Substituting eq A.5 into eq A.2, the adsorption equilibrium concentration of DCA is obtained as

$$C_{DCA_{ads}} = \frac{K_1 C_{sitesDCA,T} C_{DCA}}{1 + K_1 C_{DCA}} \quad (A.6)$$

Following the same procedure for oxygen and considering that DCA and oxygen are adsorbed on different active sites,[35] the adsorption equilibrium concentration of the oxygen can be obtained as

$$C_{O_{2ads}} = \frac{K_4 C_{sitesO_2,T} C_{O_2}}{1 + K_4 C_{O_2}} \quad (A.7)$$

A.2. Degradation Kinetic Expression for Dichloroacetic Acid

According to the mass action law and to step 2 of the reaction mechanism (Table 2), the DCA superficial reaction rate is

$$R_{Het,DCA} = -r_2 = -k_2 C_{DCA_{ads}} C_{h^+} \quad (A.8)$$

The hole superficial concentration appears in eq A.8; thus, an expression in terms of observable or measurable variables is required from the proposed reaction mechanism. Therefore, the superficial rate of appearance and disappearance of electrons is proposed, and considering the very short lifetime and very small concentration of the unstable intermediates in the unsteady-state reactor configuration, the microsteady-state approximation (MSSA) can be applied

$$r_{e^-} = r_0 - r_8 - r_9 - r_{11} = r_g - k_8 C_{e^-} C_{h^+} - k_9 C_{e^-} C_{O_{2ads}} - k_{11} C_{e^-} C_{HO_2\bullet} = 0 \quad (A.9)$$

Solving for the electron concentration in eq A.9 gives

$$C_{e^-} = \frac{r_g}{k_8 C_{h^+} + k_9 C_{O_{2ads}} + k_{11} C_{HO_2\bullet}} \quad (A.10)$$

Under the same approximation, the superficial rate of hydroperoxyl radical appearance and disappearance is

$$r_{HO_2\bullet} = r_{10} - r_{11} = k_{10} C_{O_2\bullet^-} C_{H^+} - k_{11} C_{e^-} C_{HO_2\bullet} = 0 \quad (A.11)$$

Solving for the hydroperoxyl radical concentration in eq A.11 yields

$$C_{HO_2^\bullet} = \frac{k_{10} C_{O_2^{\bullet-}} C_{H^+}}{k_{11} C_{e^-}} \quad (A.12)$$

In the same way, for the superoxide radical, one obtains

$$r_{O_2^{\bullet-}} = r_9 - r_{10} = k_9 C_{e^-} C_{O_{2ads}} - k_{10} C_{O_2^{\bullet-}} C_{H^+} = 0 \quad (A.13)$$

The superoxide radical concentration results as

$$C_{O_2^{\bullet-}} = \frac{k_9 C_{e^-} C_{O_{2ads}}}{k_{10} C_{H^+}} \quad (A.14)$$

Substituting eq A.14 into eq A.12 gives

$$C_{HO_2^\bullet} = \frac{k_9 C_{O_{2ads}}}{k_{11}} \quad (A.15)$$

Then, substituting eq A.15 into eq A.10, an expression for the electron concentration is obtained as a function of the hole concentration

$$C_{e^-} = \frac{r_g}{k_8 C_{h^+} + 2k_9 C_{O_{2ads}}} \quad (A.16)$$

Under the same assumptions, the superficial rate of hole appearance and disappearance is

$$r_{h^+} = r_0 - r_2 - r_8 = r_g - k_2 C_{DCA_{ads}} C_{h^+} - k_8 C_{e^-} C_{h^+} = 0 \quad (A.17)$$

Substituting eq A.16 into eq A.17 and using the same reasoning, we obtain

$$r_{h^+} = r_g - k_2 C_{DCA_{ads}} C_{h^+} - k_8 \frac{r_g}{k_8 C_{h^+} + 2k_9 C_{O_{2ads}}} C_{h^+} = 0 \quad (A.18)$$

Applying some algebra and solving the quadratic equation in C_{h^+}, an expression for the hole concentration that depends on DCA and oxygen concentrations is obtained as

$$C_{h^+} = \frac{2k_2 C_{DCA_{ads}} k_9 C_{O_{2ads}} \pm \sqrt{(2k_2 C_{DCA_{ads}} k_9 C_{O_{2ads}})^2 + 8 r_g k_9 C_{O_{2ads}} k_2 C_{DCA_{ads}} k_8}}{-2k_2 C_{DCA_{ads}} k_8} \quad (A.19)$$

Substituting eq A.19 into eq A.8 and choosing the negative sign of the quadratic equation solution because the reaction rate of DCA disappearance is null when there is no electron and hole generation ($r_g = 0$) then yields

$$R_{Het,DCA} = \frac{k_2 C_{DCA_{ads}} k_9 C_{O_{2ads}} - \sqrt{(k_2 C_{DCA_{ads}} k_9 C_{O_{2ads}})^2 + 2 r_g k_9 C_{O_{2ads}} k_2 C_{DCA_{ads}} k_8}}{k_8} \quad (A.20)$$

Literature Cited

(1) Hoffmann, M. R.; Martin, S. T.; Choi, W.; Bahnemann, D. W. Environmental Applications of Semiconductor Photocatalysis. *Chem. Rev.* **1995**, *95*, 69.

(2) Matthews, R. W. Photo-oxidation of Organic Material in Aqueous Suspensions of Titanium Dioxide. *Water Res.* **1986**, *20* (5), 569.

(3) Matthews, R. W. Environment: Photochemical and Photocatalytic Processes. Degradation of Organic Compounds. In *Photochemical Conversion and Storage of Solar Energy*; Pelizzetti, E., Schiavello, M., Eds.; Kluwer Academic Publishers: Amsterdam, 1991; pp 427−449.

(4) Ollis, D. F.; Pellizzetti, E. Destruction of Water Contaminants. *Environ. Sci. Technol.* **1991**, *25* (9), 1523.

(5) Goutailler, G.; Valette, J. C.; Guillard, C.; Païssé, O.; Faure, R. Photocatalyzed Degradation of Cyromazine in Aqueous Titanium Dioxide Suspensions: Comparison with Photolysis. *J. Photochem. Photobiol. A: Chem.* **2001**, *141*, 79.

(6) Topalov, A.; Molnar-Gabor, D.; Csanadi, J. Photocatalytic Oxidation of the Fungicide Metalaxyl Dissolved in Water over TiO_2. *Water Res.* **1999**, *33*, 1371.

(7) Li Puma, G.; Khor, J. N.; Brucato, A. Modeling of an Annular Photocatalytic Reactor for Water Purification: Oxidation of Pesticides. *Environ. Sci. Technol.* **2004**, *38*, 3737.

(8) Chen, D.; Ray, A. K. Photodegradation Kinetics of 4-Nitrophenol in TiO_2 Suspension. *Water Res.* **1998**, *32*, 3223.

(9) Chen, D.; Ray, A. K. Photocatalytic Kinetics of Phenol and Its Derivatives over UV Irradiated TiO_2. *Appl. Catal. B: Environ.* **1999**, *23*, 143.

(10) Sobczynski, A.; Duczmal, L.; Zmudzinski, W. Phenol Destruction by Photocatalysis on TiO_2: An Attempt to Solve the Reaction Mechanism. *J. Mol. Catal. A: Chem.* **2004**, *213*, 225.

(11) Ahmed, S.; Ollis, D. Solar Photoassisted Catalytic Decomposition of the Chlorinated Hydrocarbons Trichloroethylene and Trichloromethane. *Solar Energy* **1984**, *32* (5), 597.

(12) Calza, P. C.; Minero, C.; Hiskia, A.; Papaconstantinou, E.; Pelizzetti, E. Photocatalytic Transformations of CCl_3Br, CBr_3F, $CHCl_2Br$ and CH_2BrCl in Aerobic and Anaerobic Conditions. *Appl. Catal. B: Environ.* **2001**, *29*, 23.

(13) Stafford, U.; Gray, K.; Kamat, P. V. Photocatalytic Degradation of 4-Chlorophenol: The Effects of Varying TiO_2 Concentration and Light Wavelength. *J. Catal.* **1997**, *167*, 25.

(14) Chen, J.; Ollis, D. F.; Rulkens, W. H.; Bruning, H. Photocatalyzed Oxidation of Alcohols and Organochlorides in the Presence of Native TiO_2 and Metallized TiO_2 Suspensions. Part (II): Photocatalytic Mechanisms. *Water Res.* **1999**, *33*, 669.

(15) Chemseddine, A.; Boehm, H. P. A Study of the Primary Step in the Photochemical Degradation of Acetic Acid and Chloroacetic Acids on a TiO_2 Photocatalyst. *J. Mol. Catal.* **1990**, *60*, 295.

(16) Înel, Y.; Ökte, A. N. Photocatalytic Degradation of Malonic Acid in Aqueous Suspensions of Titanium Dioxide: An Initial Kinetic Investigation of CO_2 Photogeneration. *J. Photochem. Photobiol. A: Chem.* **1996**, *96*, 175.

(17) Dijkstra, M. F. J.; Panneman, H. J.; Winkelman, J. G. M.; Kelly, J. J.; Beenackers, A. A. C. M. Modeling the Photocatalytic Degradation of Formic Acid in a Reactor with Immobilized Catalyst. *Chem. Eng. Sci.* **2002**, *57*, 4895.

(18) Ray, A. K.; Beenackers, A. A. C. M. Novel Swirl Flow Reactor for Kinetic Studies of Semiconductor Photocatalysis. *AIChE J.* **1997**, *43* (10), 2571.

(19) Subramanian, V.; Kamat, P. V.; Wolf, E. E. Mass Transfer and Kinetic Studies during the Photocatalytic Degradation of an Azo Dye on Optically Transparent Electrode Thin Film. *Ind. Eng. Chem. Res.* **2003**, *42*, 2131.

(20) Devahasdin, S.; Fan, C.; Li, J. K.; Chen, D. H. TiO_2 Photocatalytic Oxidation of Nitric Oxide: Transient Behavior and Reaction Kinetics. *J. Photochem. Photobiol. A: Chem.* **2003**, *156*, 161.

(21) Choi, H.; Antoniou, M. G.; Pelaez, M.; De La Cruz, A. A.; Shoemaker, J. A.; Dionysiou, D. D. Mesoporous Nitrogen-Doped TiO_2 for the Photocatalytic Destruction of the Cyanobacterial Toxin Microcystin-LR under Visible Light Irradiation. *Environ. Sci. Technol.* **2007**, *41*, 7530.

(22) Gültekina, I.; Ince, N. H. Synthetic endocrine disruptors in the environment and water remediation by advanced oxidation processes. *J. Environ. Manage.* **2007**, *85* (4), 816.

(23) Marugán, J.; Hufschmidt, D.; Sagawe, G.; Selzer, V.; Bahnemann, D. Optical density and photonic efficiency of silica-supported TiO_2 photocatalysts. *Water Res.* **2006**, *40*, 833.

(24) Bahnemann, D. W.; Kholuiskaya, S. N.; Dillert, R.; Kulak, A. I.; Kokorin, A. I. Photodestruction of dichloroacetic acid catalyzed by nanosized TiO_2 particles. *Appl. Catal. B: Environ.* **2002**, *36*, 161.

(25) Lindner, M.; Bahnemann, D. W.; Hirthe, B.; Griebler, W. D. Solar water detoxification: Novel TiO_2 powders as highly active photocatalysts. *J. Sol. Energy Eng.* **1997**, *119*, 120.

(26) Bahnemann, D.; Hilgendorff, M.; Memming, R. Charge Carrier Dynamics al TiO_2 Particles: Reactivity of Free and Trapped Holes. *J. Phys. Chem.* **1997**, *101*, 4265.

(27) Bahnemann, D. Photocatalytic Detoxifications of Polluted Waters. In *The Handbook of Environmental Chemistry*; Springer-Verlag: Berlin, 1999; Vol. 2, Part L: Environmental Photochemistry.

(28) Zalazar, C. S.; Romero, R. L.; Martín, C. A.; Cassano, A. E. Photocatalytic Intrinsic Reaction Kinetics I: Mineralization of Dichloroacetic Acid. *Chem. Eng. Sci.* **2005**, *60*, 5240.

(29) Satuf, M. L.; Brandi, R. J.; Cassano, A. E.; Alfano, O. M. Experimental Method to Evaluate the Optical Properties of Aqueous Titanium Dioxide Suspensions. *Ind. Eng. Chem. Res.* **2005**, *44*, 6643.

(30) Satuf, M. L.; Brandi, R. J.; Cassano, A. E.; Alfano, O. M. Quantum Efficiencies of 4-Chlorophenol Photocatalytic Degradation and Mineralization in a Well-Mixed Slurry Reactor. *Ind. Eng. Chem. Res.* **2007**, *46*, 43.

(31) Satuf, M. L.; Brandi, R. J.; Cassano, A. E.; Alfano, O. M. Photocatalytic Degradation of 4-chlorophenol: A Kinetic Study. *Appl. Catal. B: Environ.* **2008**, *82*, 37.

(32) Ballari, M. M.; Brandi, R. J.; Alfano, O. M.; Cassano, A. E. Transfer Limitations in Photocatalytic Reactors Employing Titanium Dioxide Suspensions: I. Concentration Profiles in the Bulk. *Chem. Eng. J.* **2008**, *136*, 50.

(33) Ballari, M. M.; Brandi, R. J.; Alfano, O. M.; Cassano, A. E. Transfer Limitations in Photocatalytic Reactors Employing Titanium Dioxide Suspensions: II. External and Internal Particle Constrains for the Reaction. *Chem. Eng. J.* **2008**, *136*, 242.

(34) Wolf, K.; Bockelmann, D.; Bahnemann, D. Mechanistic Aspects of Chemical Transformations in Photocatalytic System. In *Symposium on Electronic and Ionic Properties of Silver Halides: Common Trends with Photocatalysis. Proceedings of the IS&T 44th Annual Conference*; Levt, B., Ed.; IS&T: Springfield, VA, 1991; pp 259−267.

(35) Turchi, C. S.; Ollis, D. F. Mixed Reactant Photocatalysis: Intermediates and Mutual Rate Inhibition. *J. Catal.* **1990**, *122* (1), 178.

(36) Alfano, O. M.; Cabrera, M. I.; Cassano, A. E. Photocatalytic Reactions Involving Hydroxyl Radical Attack. I. Reaction Kinetics Formulation with Explicit Photon Absorption Effects. *J. Catal.* **1997**, *172*, 370.

(37) Sagawe, G.; Brandi, R. J.; Bahnemann, D.; Cassano, A. E. Photocatalytic Reactors for Treating Water Pollution with Solar Illumination. I: A Simplified Analysis for Batch Reactors. *Chem. Eng. Sci.* **2003**, *58*, 2587.

(38) Sagawe, G.; Brandi, R. J.; Bahnemann, D.; Cassano, A. E. Photocatalytic Reactors for Treating Water Pollution with Solar Illumination. II: A Simplified Analysis for Flow Reactors. *Chem. Eng. Sci.* **2003**, *58*, 2601.

(39) Özisik, M. N. *Radiative Transfer and Interactions with Conduction and Convection*; Wiley: New York, 1973.

(40) Cassano, A. E.; Martín, C. A.; Brandi, R. J.; Alfano, O. M. Photoreactor Analysis and Design: Fundamentals and Applications. *Ind. Eng. Chem. Res.* **1995**, *34*, 2155.

(41) Alfano, O. M.; Cabrera, M. I.; Cassano, A. E. Modeling of Light Scattering in Photochemical Reactors. *Chem. Eng. Sci.* **1994**, *49*, 5327.

(42) Siegel, R.; Howell, J. R. *Thermal Radiation Heat Transfer*; Hemisphere Publishing Corp.: Bristol, PA, 2002.

(43) Van de Hulst, H. C. *Multiple Light Scattering*; Academic Press: New York, 1980.

(44) Duderstadt, J.; Martin, W. *Transport Theory*; Wiley: New York, 1979.

(45) Murov, S.; Carmichal, I.; Hayon, E. *Handbook of Photochemistry*; Marcel Dekker: New York, 1993.

(46) Zalazar, C. S.; Labas, M. D.; Martín, C. A.; Brandi, R. J.; Alfano, O. M.; Cassano, A. E. The Extended Use of Actinometry in the Interpretation of Photochemical Reaction Engineering Data. *Chem. Eng. J.* **2005**, *109*, 67.

(47) Brandi, R. J.; Citroni, M. A.; Alfano, O. M.; Cassano, A. E. Absolute Quantum Yields in Photocatalytic Slurry Reactors. *Chem. Eng. Sci.* **2003**, *58*, 979.

Received for review August 3, 2008
Revised manuscript received November 20, 2008
Accepted November 25, 2008

IE801194F